Noname manuscript No.
(will be inserted by the editor)

The Application of Mechanistic Cutting Force Models for Deburring

Grael Miller · Mojtaba Ahmadi · Rishad Irani

Received: date / Accepted: date

Abstract In this paper, the performances of two cutting force models are compared alongside two methods for identifying their empirical parameters. The models' performances are evaluated with the aim of determining which model is suited to the prediction of forces generated during the operations with features sizes less than 1 *mm*. The models' empirical parameters were then identified using a linear regression on collected force data and a simplex search-based optimization method that minimized the error between the model output and the measured data. The models' predictions were compared to experimental results gathered from several shallow milling passes conducted at a variety of tool immersions. The models were used to produce force estimates based on measured milling parameters and depth of cut estimates based on the measured forces. The simplex search method was shown to be the most effective of the identification techniques. In full immersion tests, the linear model trained using the linear regression method performed best. However, in low MRR partial immersion tests, which more closely resemble deburring operations, the exponential model trained via simplex search outperformed the linear model by nearly two orders of magnitude.

Keywords cutting force model · nonlinear force model · Milling · deburring

1 Introduction

Deburring is a ubiquitous finishing process in the manufacture of metal and composite parts, accounting for approximately 9% of total manufacturing costs [1]. A large portion of deburring is performed by hand, exposing workers to sharp edges and metal dust. Automating the process through robotic deburring is an appealing solution, as robotic manipulators can be made cheaper and can cover a larger work volume than traditional CNC centres. The added flexibility and lower cost of robotic manipulators comes at the cost of lower rigidity and precision. Additionally, the low contact forces generated by low material removal rate (MRR) operations such as deburring significantly decrease the signal to noise ratio. To compensate for the lower rigidity of robotic manipulators and the increased noise on the feedback signal, it is necessary to develop robust control solutions to ensure a consistent finished edge.

To design an effective controller for the deburring process, it is important to be able to model the forces generated through deburring. In the literature, deburring modelling is primarily focused on simple empirical models for use as part of a force control solution. For example Her and Kazerooni [2] propose a very simple relationship wherein the tangential force is directly related to the cutting force by

$$F_t = K \times MRR \tag{1}$$

where K is an experimentally determined constant and MMR is the material removal rate in grams per second. Hsu and Fu [3] propose a contact model based on the tool position relative to the edge. A number of proposed deburring solutions do not consider the contact force explicitly; instead, they experimentally determine the cutting force required to achieve a desired finished surface [4,5]. The disadvantage to implicitly considering the contact force in this way is that a new "ideal" contact force must be determined for each new tool workpiece combination as well as for each new desired surface finish.

While a great deal of scientific effort has been applied to model the cutting of metal, to the best knowledge of the authors at this time, existing metal cutting models have not been applied to the problem of deburring. The purpose of

G. Miller
Tel.: +289 387 0214
E-mail: graelmiller@cmail.carleton.ca

this paper is to begin the investigation into the application of existing cutting models to the task of predicting the cutting forces during low MRR operations such as deburring. These models are important as they could be used in two ways: the first use is as a pre-processing algorithm that predicts the forces created by the deburring operation where the models are used to generate an acceptable and/or optimal toolpath. The model's second purpose is as an on-line observer to provide an estimate of the depth of cut, material removal rate and contact forces that will be used in real-time control of the tool path to maintain a consistent and accurate finish.

As a pre-process step, the model should be able to accurately predict the forces generated during the finishing operation when given an accurate measurement of the volume and position of the features to be removed. The forces predicted by the model can then be used to plan optimal toolpaths to maximize the throughput for the system. Additionally, the predicted forces could be passed to the force controller to maintain the desired contact force at each point along the toolpath.

The model's secondary purpose is to serve as an on-line observer of the depth of cut. While the robot is in operation, it will not be possible to measure the depth of cut directly without stopping the spindle. Using the robot's forward kinematics, the CAM information of the workpiece, and the geometry of the tooling it will be possible to estimate the depth of cut; however, a purely kinematic strategy for depth of cut estimation is prone to measurement noise and errors in the accuracy of the robot's kinematic model. As an observer, the model can provide a second estimate of the depth of cut using the measured forces online, while attempting to maintain a desired contact force.

This paper investigates the accuracy of existing cutting force models developed for conventional scale milling when used to predict the forces generated by high speed, low material removal rate operations found in deburring. The deburring process approaches the boundary of what is considered micro-scale machining, so it is possible that some of the effects that dominate machining forces at that scale could cause inaccuracies in the existing cutting models.

This paper is divided into seven sections. The first being this brief introduction to the paper and its contents. The second section gives background on the mechanistic cutting force models used in this paper. The third section contains a brief overview of the derivation of the equations used in this paper from the base model. The fourth section outlines the equipment and procedures used to collect the data. Section five presents the two methods used to identify the empirical parameters of the models, while the last two sections summarize the results and provide conclusions respectively.

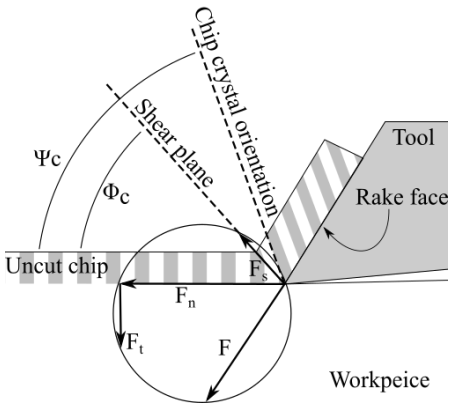

Fig. 1 Merchant circle showing the force relationships of an orthogonal cut. Adapted from [7]

2 Background

From the middle of the 20^{th} century to the present, a great deal of scientific effort has been devoted to the accurate predictions of the forces generated during machining. In general the cutting-force models found in literature can be placed in three categories: analytical, finite element methods (FEM), and mechanistic. While mechanistic models were selected to form the basis of the deburring models, it is useful to have a basic understanding of the current state of the art of cutting force modelling. The following is a brief review of existing orthogonal cutting models.

2.1 Analytical Models

Analytical models predict the forces and material deformation generated through cutting by using relationships derived from physics and solid mechanics. The analytical model, proposed by Merchant [6], is among the earliest attempts to model the cutting process scientifically. Figure 1 shows a diagram of the basic elements of the Merchant model which breaks the resultant cutting force F into the easier-to-measure normal and tangential components F_T and F_N which are then related to the work performed across the shear plane Φ_c to deform the structure of the uncut chip into the cut chip with crystal orientation Ψ_c as well as the measured shear force F_s. The model assumes an ideal isotropic material with perfectly rigid-plastic behaviour with no temperature or strain hardening effects considered. The omission of strain hardening caused poor agreement with experimental data [7].

The Merchant model was improved by Palmer and Oxley [7] who replaced the 2D shear plane with a zone of plastic deformation. The model proposed by Palmer and Oxley uses lines of constant shear and hydrostatic stress, slip-lines, to provide a more accurate picture of how the metal is being deformed through the entire plastic region. The slip-line model also allowed for the inclusion of work-hardening

terms omitted by the Merchant model which improved the model's agreement with experimental results [7].

The slip-plane model was further improved by Roth and Oxley [8] to include the secondary shear zone along the rake face of the tool, noted in Figure 2. The improved slip-line model also accounted for the curl in the produced chip by modelling the elastic contact between the rake face of the tool. The universal slip-line model developed by Fang et al. [9] combines the work of Oxley and Palmer to create a slip-line model that predicts not only contact forces and shear stress but chip curl radius and the flow of material under the tool tip among others.

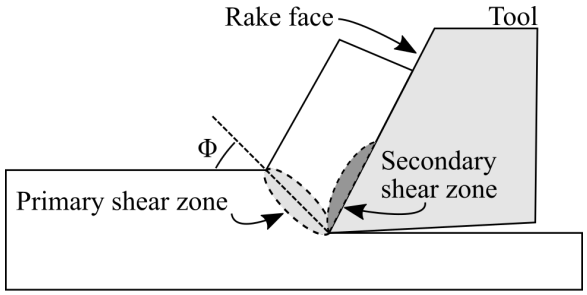

Fig. 2 Simplified locations of shear zones in chip formation during orthogonal cut.

While the current analytical models show good agreement with experimental data [9] they are very complex to implement. Current analytical models are dependent on very accurate measures of the material properties and geometry of the tool and workpiece, which can be difficult to measure accurately [9,10]. These models are designed to be of use for the development of more efficient machine tooling and strategies [6,8,9]. Additionally, the quantities the analytical models predict, chip curl radius and shear-plane angle are not useful for the proposed deburring model. As computational power becomes cheaper and easier to access more research has been focused on creating finite element models that can take better advantage of that power.

2.2 Finite element methods

Finite element method (FEM) models attempt to simulate the actual behaviour of the cutting process. In an FEM model the workpiece and tool are broken up into a mesh of small elements which are connected following a simplified analytical model. FEM models provide highly detailed information about the behaviour of the chip during the cutting process [10], however, they are highly dependent on the boundary conditions and the selection of the physical parameters such as yield stress and friction coefficients [11]. The acquisition of these physical parameters can be very difficult in the case of cutting models where strains and strain rates are much higher than what can be measured experimentally [12]. As with the analytical models discussed previously, FEM models also model a number of chip behaviours that are of little to no use for deburring applications. FEM models are also computationally much more expensive to run which makes them poorly suited for online applications [10][11]. Unlike the analytical and FEM models mechanistic models are simple to implement, accurate and are typically very computationally efficient.

2.3 Mechanistic Force Models

Mechanistic models typically consist of a function whose form is taken from analytical models with one or more lumped empirical coefficients. The empirical coefficients combine the effects of the physical properties of the tool and workpiece into a single value. The empirical coefficients are only applicable for the specific tool workpiece combination they are trained for, meaning the experimentally determined constants must be re-calculated with each new tool workpiece combination.

An early mechanistic force model was proposed by Sabberwall and Koensbeurger [13] who proposed a direct proportionality K_t between the tangential cutting force F_t and the uncut chip area ha as well as a direct proptionality K_c between the tangent force and the cutting force F_c

$$F_t = K_t h a, \tag{2}$$

$$F_c = K_c F_t, \tag{3}$$

where h is the uncut chip thickness and a is the axial depth of cut and K_t and K_c are empirically determined constants. The Koensbeurger model was further improved by Altintas and Budak [14]. The Altintas model proposes a linear relationship between the instantaneous chip thickness h and cutting forces

$$F_j = (K_{jc} h + K_{je}) a \qquad j \in t,r,a \tag{4}$$

where t,r,a represent the tangential, radial and axial directions respectively, h is the instantaneous uncut chip thickness and a is the axial depth of cut, K_{tc}, K_{rc}, K_{ac} are the empirical parameters that represent the forces generated by the mechanical shearing of the metal and K_{te}, K_{re}, K_{ae} are empirical parameters that represent the forces generated by all sources of friction independent of the cutting action such as ploughing and edge rubbing [15].

Another popular mechanistic model in the literature is the exponential model proposed by Keinzel [16]. The exponential model proposes an exponential relationship between the cutting forces and the uncut chip thickness as

$$F_j = K_j a h^{\beta} \qquad j \in t,r,a, \tag{5}$$

where K_t, K_r, K_a and β are the lumped empirical coefficients. The Keinzel model is less commonly used due in part to its non-linearity. However, with current computing technology, the model can be evaluated in real time and the few papers that have used the model showed results that were comparable to or surpassed the accuracy of the Altintas model [16, 17, 18].

While the Altintas and Keinzel models are common in literature, there have been attempts at constructing other mechanistic models based on other cutting parameters. For example, Auerbach et al. propose a model that makes use of machining variables that are more readily measured by existing process control systems in industry [19]. The Auerbach model proposes a relation between the cutting area and the milling force F_a such that

$$F_A = c_1 + \frac{c_2 bah}{bc_3}, \tag{6}$$

where $c_{1,2,3}$ are empirical parameters and b is the width of cut. However, as noted by Zhang et al. [20] models that consider the instantaneous uncut chip thickness explicitly as part of the model outperform those that do not. The importance of considering the uncut chip thickness directly helps to explain the lasting impact and continued use of the Altintas and Keinzel models. In addition to the structure of the models themselves, a great deal of effort has gone into the fast and accurate computation of the empirical parameters.

2.3.1 Parameter identification

Budak and Altintas provided a method to identify the parameters from orthogonal cutting data [21]. Altintas et al. propose the creation of a database of physical parameters based on numerous experiments, so that physical parameters of any given tool-workpiece combination could be looked up and used to compute a set of matching empirical parameters. Altintas outlines another method for obtaining the coefficients through linear regression [15]. The linear regression method uses a number of single feed rate tests to identify the the parameters, the method is effective but time consuming. Adem et al. propose a global optimization solution in which a large set of cutting data is used to train the coefficients simultaneously using a simplex search algorithm [16]. The proposed simplex search allows for more efficient traininmg of the model compared to the linear as it allows for a wider variety of data to be included in the training, however in Adem et al. it was only tested on full immersion data.

Shwenzer et al.[17, 18] proposes using an online optimization algorithm to continuously update the parameters as they change due to cutter wear and other environmental factors. The work by Shwenzer includes the comparison of a large variety of existing local and global solvers [17] and an application of the ensemble Kalman filter [18]. Online optimization methods have some potential drawbacks as the system is under-constrained which can lead the global solvers to converge to different local solutions if their initial conditions were not set carefully [17]. The results of these online strategies are very appealing from an industrial standpoint as they remove one of the primary drawbacks of the mechanistic models which is the time required to train the model for each new tool-workpiece interaction.

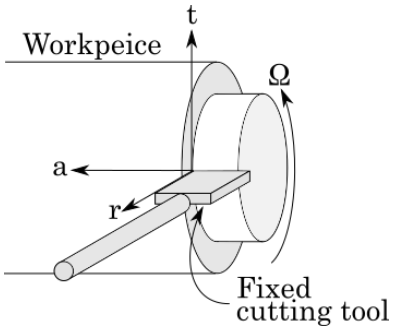

Fig. 3 Alignment of tool coordinate frame for single point turning operation

Mechanistic models, specifically the linear model proposed by Altintas and the nonlinear model proposed by Keinzel, which are the most widely used in the literature, were selected as the basis functions of the deburring model. Mechanistic models were selected as they are the most computationally efficient, they have good agreement with experimental results and unlike the analytical and FEM models do not output extraneous information [16, 15, 17].

3 Model form

The linear model of Altintas and Budak and nonlinear force model by Keinzle used in this research were developed to model single point cutting operations; Figure 3 shows a simplified diagram of a single point turning operation. In Figure 3 coordinate frame is defined with its origin fixed cutting edge with three orthogonal axes: radial, tangential, and axial noted as r, t, and a. In a fixed point operation, the cutting edge is fixed and held orthogonal to the part and the workpiece is moved relative to the cutting edge. During a fixed point cut, the chip thickness h_{fp} is constant with

$$h_{fp} = \frac{V_a}{\Omega}$$

and depends only on the linear feed rate in the axial direction V_a and the angular velocity of the spindle Ω . Although the models' forms are derived from fixed point operations they remain valid for any orthogonal cutting element.

The Altintas model proposes a linear relationship between the instantaneous chip thickness h and the instanta-

neous cutting forces are governed by six empirical parameters such that

$$F_t = (K_{tc}h + K_{te})a \tag{7}$$
$$F_r = (K_{rc}h + K_{re})a \tag{8}$$
$$F_a = (K_{ac}h + K_{ae})a \tag{9}$$

where $F_{t,r,a}$ are the instantaneous force in the tangential, radial and axial direction respectively, h is the instantaneous uncut chip thickness and a is the axial depth of cut, $K_{(t,r,a)c}$ and $K_{(t,r,a)c}$ are the six lumped empirical parameters.

Kienzle's non-linear model proposes an exponential relationship between the feed per tooth and the cutting forces, and is governed by only four empirical parameters such that

$$F_t = K_t a h^{\beta} \tag{10}$$
$$F_r = K_r a h^{\beta} \tag{11}$$
$$F_a = K_a a h^{\beta} \tag{12}$$

where h and a represent the instantaneous chip thickness and axial depth of cut respectively, $K_{t,r,a}$ are axis specific empirical parameters and β which is an empirical parameter common to all three axes [22].

As discussed earlier, the empirical parameters in both the linear and non-linear models are lumped parameters that replace a more complex analytical function and are directly obtained experimentally by observing the cutting forces. It is, possible to fit these parameters by using analytical models that relate other cutting quantities such as rake angle and shear plane angle to the cutting parameters [21]. However, obtaining the parameters analytically is difficult as it requires the ability to observe the chip formation directly in order to measure the shear plane angle and very accurate measurement of the material properties of the workpiece. The model is only valid for orthogonal cuts, therefore, to apply the model to the curved cutting edge found on a typical helical end-mill the cutting edge must be discretized.

Figure 4 shows a diagram of the discretization of a standard 2 flute helical end mill. The end-mill is discretized along the Z-axis of the tool, creating j elements of height dz with i orthogonal teeth per cutting element where i is the number of flutes in the cutter. Each of these cutting elements is offset from the previous element by angle ψ given as

$$\psi = \frac{2\tan(\delta)}{D} dz \tag{13}$$

where δ is the helix angle of the tool and D is the tool diameter. The larger the value of δ the more elements j are required to avoid numerical errors [15].

Since the milling operation is intermittent, with each tooth following a trochoidal path through the material, the chip thickness is not dependant only on feed rate but also includes a dependency to the rotation angle of the cutter ϕ. The chip

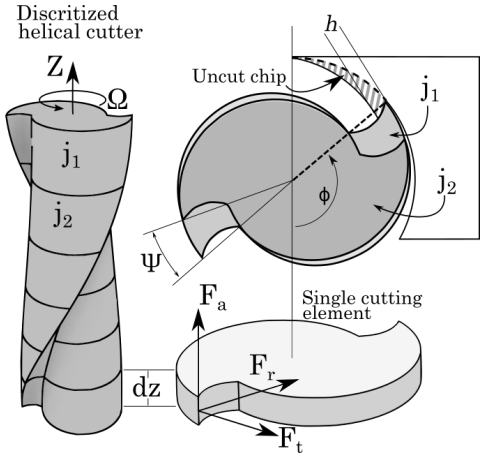

Fig. 4 Left: Diagram of discretized two flute end mill. Upper right: Angular offset Ψ between each cutting element. Lower right: Coordinate frame location for single cutting element.

thickness for a given tooth i of the j^{th} cutting element is given by

$$h_{i,j} = f \sin(\phi_{i,j}), \tag{14}$$

where f is the feed per tooth in $\frac{mm}{rev \times tooth}$ and $\phi_{i,j}$ is the immersion angle of the i^{th} tooth of the j^{th}cutting element is

$$\phi_{i,j} = \phi + \frac{2\pi}{N} i + \psi j, \tag{15}$$

where ϕ is the immersion angle of the first tooth of the first cutting element, N is the number of teeth per cutting element. It should be noted that (14) is a chip thickness formula that does not account for cutter run-out and tool deflection. For the linear model substituting the instantaneous chip thickness of the i^{th} tooth of the j^{th} cutting element $h_{i,j}$ into (7) through (12) yields

$$dF_{n_{j,i}} = (K_{nc}h_{i,j} + K_{ne})dz \qquad n \in t,r,a \tag{16}$$

and for the exponential model,

$$dF_{n_{j,i}} = K_n h_{i,j}^{\beta} dz \qquad n \in t,r,a \tag{17}$$

where in both cases $dF_{n_{j,i}}$ is the force in the n-axis for the i^{th} tooth of the j^{th} cutting element. In order to model the forces generated by the whole tool, the forces from each cutting element are transformed from their local edge frame (t,r,a) into the tool frame (x,y,z) with a transformation matrix such that

$$\begin{Bmatrix} dF_x \\ dF_y \\ dF_z \end{Bmatrix} = \begin{bmatrix} -\cos\phi_{i,j} & -\sin\phi_{i,j} & 0 \\ \sin\phi_{i,j} & -\cos\phi_{i,j} & 0 \\ 0 & 0 & 1 \end{bmatrix} \begin{Bmatrix} dF_t \\ dF_r \\ dF_a \end{Bmatrix}, \tag{18}$$

where the x-axis is along the direction of cut, the y-axis is normal to the cut and the z-axis is along the tool axis. The

transformation matrix also contains a reflection about the X-axis and Y-axis to align with existing conventions for milling forces. After applying (18) the cutting elements share a common coordinate frame the forces can be integrated along the z-axis such that

$$F_n = \int_0^z dF_n(\phi_{i,j},z)dz \qquad n \in x,y,z, \tag{19}$$

where F_n is the instantaneous force in the n direction as a function of the immersion angle ϕ and the feed per tooth where $n = x,y,z$. The axial integration can be done analytically or numerically depending on the geometry of the cutting tool.

In order to obtain the average force $\bar{F}_n$, the instantaneous force is integrated over one full revolution of the cutter. Figure 5 shows the definition of the limits of integration ϕ_{st} and ϕ_{ex} which are the immersion angles where the cutter enters and leaves the workpiece respectively. With the limits of integration defined, the mean force $\bar{F}_n$ is given as

$$\bar{F}_n = \frac{N}{2\pi}\int_{\phi_{st}}^{\phi_{ex}} F_n d\phi \qquad n \in x,y,z. \tag{20}$$

To simplify the equations further, if the tool is fully immersed in the part (ie. $\phi_{st} = 0$ and $\phi_{ex} = pi$), then average force per cutter revolution $\bar{F}$ for the linear model is given by [16]

$$\bar{F}_x = \left(\frac{-NK_{rc}}{4}f - \frac{NK_{re}}{\pi}\right)a, \tag{21}$$

$$\bar{F}_y = \left(\frac{NK_{tc}}{4}f + \frac{NK_{te}}{\pi}\right)a, \tag{22}$$

$$\bar{F}_z = \left(\frac{NK_{ac}}{\pi}f + \frac{NK_{ae}}{2}\right)a, \tag{23}$$

$$\tag{24}$$

which has an analytical solution. For the exponential model, whose integral must be solved numerically, the mean force is given by

$$\bar{F}_x = \frac{Na}{2\pi}K_r f^\beta \int_0^\pi \sin^\beta\theta \sin\theta d\theta, \tag{25}$$

$$\bar{F}_y = \frac{Na}{2\pi}K_t f^\beta \int_0^\pi \sin^\beta\theta \sin\theta d\theta, \tag{26}$$

$$\bar{F}_z = \frac{Na}{2\pi}K_a f^\beta \int_0^\pi \sin^\beta\theta d\theta. \tag{27}$$

With the models in this form they can be used more easily identify the empirical parameters using data collected using the experimental testbed.

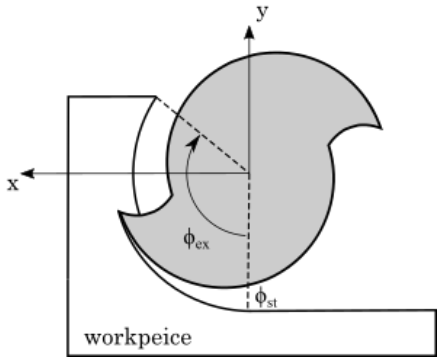

Fig. 5 Immersion angle measurement for up milling cut

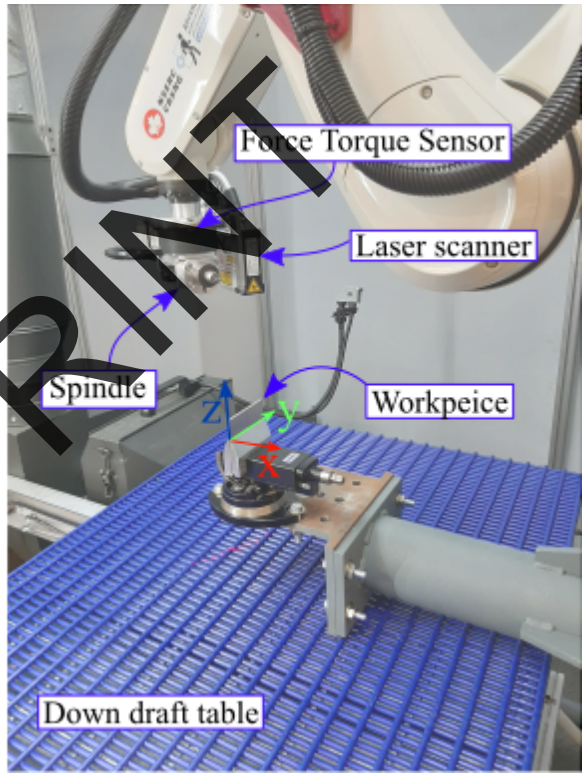

Fig. 6 Photo of robotic tested and location of world frame coordinate system.

4 Experimental testbed

To begin the identification of the models' empirical parameters, a number of tests were conducted where a slot was cut out of a coupon of aluminum 6061. The slot for each test was 63.5mm long with a commanded depth of 0.5 mm. For all the tests a 1/8 inch 2 flute flat end carbide end mill was used. Figure 6 shows the experimental setup, the endmill is driven by a 350 W electric spindle mounted on a 6-DOF robotic manipulator. A force torque sensor was mounted between the spindle and the last joint of the robot to measure the contact force in the tool frame. Two sets of data were collected, one set where the feed per tooth was kept constant for

the whole test and a second set where the feed per tooth was linearly increased throughout the slot. Table 1 provides the spindle rpm and linear feed rate used in each of the tests, as well as the resultant feed per tooth. In tests where a the feed rate was varied linearly along the cut the start and end feed rate are listed.

Table 1 Test plan for gathered full immersion experimental data

spindle speed $[krpm]$	feed rate $\left[\frac{mm}{s}\right]$	fpt $\left[\frac{mm}{rev\ tooth}\right]$
15	1	0.002
10	1	0.003
5	1	0.006
15	2	0.004
10	2	0.006
20	3	0.0045
15	3	0.006
10	3	0.009
20	4	0.006
15	4	0.008
10	4	0.012
20	5	0.0075
15	5	0.01
10	5	0.015
20	5.5	0.00825
15	5.5	0.011
20	$1 \rightarrow 5$	$0.0015 \rightarrow 0.0075$
15	$1 \rightarrow 5$	$0.002 \rightarrow 0.01$
10	$1 \rightarrow 5$	$0.0015 \rightarrow 0.0075$
20	$1 \rightarrow 10$	$0.0015 \rightarrow 0.0015$
15	$1 \rightarrow 10$	$0.002 \rightarrow 0.02$
20	$1 \rightarrow 20$	$0.0015 \rightarrow 0.03$

Additionally, to aid in the parameter identification and overall quantification of the cut, each cut slot was scanned using a laser profile scanner to obtain the depth of cut along the slot.

5 Parameter identification

The data collected from the testbed can now be used to identify the empirical parameters using the linear regression method outlined by Altintas [15] and the simplex search method outlined by Adem [16]. The linear regression method, Section 5.1, makes use of only the constant feed-rate tests while the simplex search method, Section 5.2, is able to make use of all the collected data.

5.1 Linear regression method

The linear regression method outlined by Altintas identifies the empirical parameters by plotting the mean force of each test against its feed rate, the slope and y-intercept of the measured data can be used to identify the empirical parameters in (21) – (27).

In order to use the expressions for mean force presented in equations (21) – (27) to identify the model parameters they had to be modified slightly. In equations (21) – (27) the mean force is dependent on the depth of cut a which is assumed to be constant throughout the cut. However, in practice it was not possible to maintain a constant depth of cut throughout each test. To eliminate the need to maintain a constant depth of cut, the depth was divided out of both sides of the equations such that the model now relates the specific force F_{sn} to the feed per tooth where the specific force is defined as

$$F_{sn} = \frac{F_n}{a}. \tag{28}$$

The final form of the linearized model used to fit the measured data is

$$\bar{F}_{sx} = \frac{-NK_{tc}}{4} f - \frac{NK_{re}}{\pi} \tag{29}$$

$$\bar{F}_{sy} = \frac{NK_{tc}}{4} f + \frac{NK_{te}}{\pi} \tag{30}$$

$$\bar{F}_{sz} = \frac{NK_{ac}}{\pi} f + \frac{NK_{ae}}{2}. \tag{31}$$

Additionally, the log of both sides of the exponential model (25) – (27) is taken to transform the exponential relationship into the following linear equation

$$\ln(\bar{F}_{sx}) = \beta \ln(f) + \ln\left(\frac{N}{2\pi} K_r \int_0^{\pi} \sin^{\beta}\theta \sin\theta d\theta\right) \tag{32}$$

$$\ln(\bar{F}_{sy}) = \beta \ln(f) + \ln\left(\frac{N}{2\pi} K_t \int_0^{\pi} \sin^{\beta}\theta \sin\theta d\theta\right) \tag{33}$$

$$\ln(\bar{F}_{sz}) = \beta \ln(f) + \ln\left(\frac{N}{2\pi} K_a \int_0^{\pi} \sin^{\beta}\theta \sin\theta d\theta\right). \tag{34}$$

Once the models have been transformed into a linear form the next step is to use experimental data to fit the empirical parameters using linear regression.

For the X,Y and Z-axes, figure 7 and 8 show the the measured specific mean force as a function of measured feed per tooth and the natural log of the measured specific force as a function of the natural log of the measured feed per tooth respectively, alongside their respective linear trend lines. Figure 7 and 8 have linear correlation coefficient of $R = .95$ between the feed per tooth and the specific mean force along the Y-axis. The forces generated along the X-axis, show a lower linear correlation, R = 0.82 for the linear and R = 0.75 for the exponential model, which is more pronounced at feed rates below $0.008\ \frac{mm}{rev \times tooth}$.

The cause of the variability of the force along the X-axis feed rates below $\frac{mm}{rev \times tooth}$ is likely due to the increased forces along the X-axis creating larger vibrations in the robotic

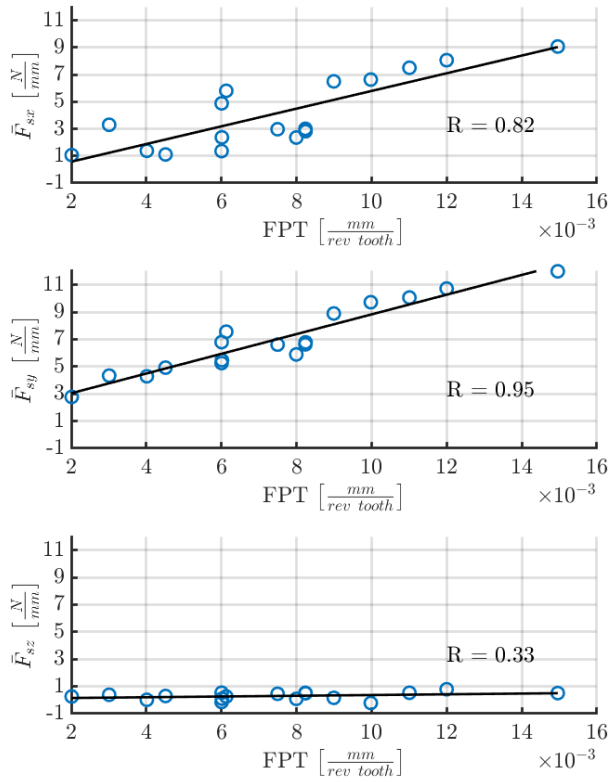

Fig. 7 Linear model training set: Specific mean cutting force vs. feed per tooth

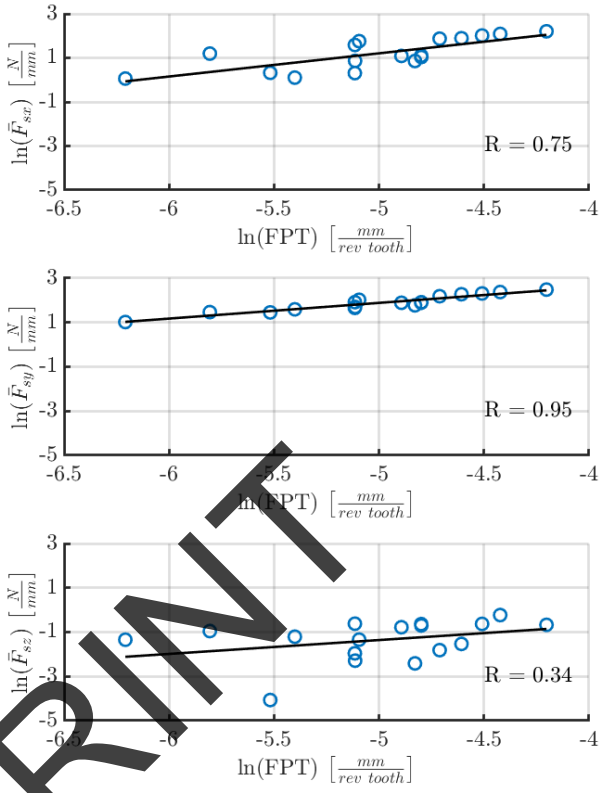

Fig. 8 Exponential model training set: natural log of specific mean cutting force vs. natural log of feed per tooth

manipulator. The forces along the z-axis show the weakest correlation with R=0.33, which is most likely due to a combination of the contact forces below $1N$ measured in the Z-axis along with the fact that it is most affected by the vibration of the workpiece. The Z-axis is typically omitted from models since it has little effect on control or process modelling. Thus, the remainder of the current study is focused on the X and Y-axis forces.

Table 2 collects the identified parameters of the linear and exponential models, respectively. The identified parameters follow the general trends of these coefficients that $K_t > K_r > K_a$, found in other papers where similar identification procedures were conducted [23,16]. The only major difference between the results and those presented in the literature being the much lower values for K_{ne} which are the y-intercept values for the model. The low y-intercept values imply that at the $1000:1$ ratio of rpm to linear feed rate reached during the tests, the friction terms are almost negligible relative to the shearing forces. As an alternative to the linear regression method, following the work presented by Adem [16], the parameters were also identified using the simplex search method.

5.2 Simplex search method

The simplex search method allows for the whole data set to be considered at once not just a single average force from each test. In addition to considering a whole data set at once, the feed rate can be varied throughout each trial. The ability to vary the feed rate throughout each trial allows for a much wider range of feed rates to be collected in fewer trials. For the specific set-up used in these experiments it allowed for much higher feed rates since the feed rate could start slow at around 1 *mm* per second and build to a speeds in excess of 20 *mm* per second without stalling the tool.

The data was prepared by trimming the transients from the force data, then combining the force, depth, and feed per tooth data of each test into a single dataset. The MATLAB implementation of the simplex search function `fminsearch` was used to minimize the cost function C, where

$$C = \frac{1}{n}\sum(|F_{mes} - F_{pred}|)^2 \tag{35}$$

where F_{mes} is the measured force and F_{pred} is the force predicted by the model and n is the number of samples taken. Table 2 summarizes the cutting parameters identified using the search method and linear regression for both models. The simplex search method allows for much wider ranges

of feed rates to be added to the training set with far fewer trials. For example, by observing table 1 you can see that the first three variable feed rate tests cover nearly the entire set of feedrates covered by the first fifteen single feed rate tests which makes it much more time efficient to train the model using the simplex search method.

6 Results

Once the model parameters were identified, their performances were evaluated by comparing the forces predicted by the model to those gathered experimentally. Table 3 collects the mean error for each training method. There is less than 1 N of absolute error across all training methods, with the exception of the exponential model trained using the linear regression method which produced a mean error of 2.95 N. Furthermore, Table 3 shows that the two best performing models are the linear model trained using linear regression and the exponential model trained using the simplex search method.

In Figure 9, where the left side uses the linear regression, the right side uses the simplex search method, the X and Y-axis forces predicted by the linear and exponential models are plotted against the feed per tooth as dashed and solid lines respectively along with the measured force represented by the blue lines. The Y-axis forces predicted by the exponential model trained via linear regression in Figure 9 are significantly under-predicting the measured forces. In the second column of Figure 9 both the linear and exponential model have essentially the same form as the exponential model except for better performance from the exponential model predicting the X-axis forces at higher feedrates.

6.1 Depth estimation

In addition to predicting the cutting forces generated, the deburring force model is intended to work as an observer by taking in force measurements and returning a predicted depth of cut. To test the models' performances as an observer, the error in the force prediction was run through the model restructured to output the estimated depth error a_n for the linear model such that

$$a_n = \frac{|\bar{F}_n - F_{mes}|}{\frac{-NK_{nc}}{4} f - \frac{NK_{ne}}{\pi}} \tag{36}$$

and for the exponential model

$$a_n = \frac{|\bar{F}_n - F_{mes}|}{\frac{N}{2\pi} K_r f^{\beta} \int_0^{\pi} \sin^{\beta}\theta \sin\theta d\theta}, \tag{37}$$

Table 4 shows the mean estimated depth error plus or minus two standard deviations. When using the metric of estimated depth error to compare the models, the linear model outperforms the exponential model by more than 3 times with a mean depth error of -0.011 ± 0.17 *mm* compared to the exponential model's mean error of 0.035 ± 0.25 *mm*.

Figure 10 shows the estimated depth prediction error plotted against the measured feed per tooth using the linear regression and simplex search method for both the linear and exponential models. The exponential model shows better agreement at feed-rates exceeding 0.01 $\frac{mm}{rev \times tooth}$. Despite both of the models omitting tool run-out, plastic deformation and the chip size effect, which has been shown to have a larger effect at feedrates below $< 0.1 \frac{mm}{rev \times tooth}$[16], both models have mean depth estimation error approaching or below the 0.03 mm repeatability of the robotic manipulator uses to carry out the experiments.

6.2 Model training results

Of the two training methods tested, the simplex search method produced the best results overall, with a mean force estimation error of 0.34 N across both models compared to the linear regression model's 0.67 N. However, observing the first row of Tables 3 and 4, the performance of the linear model is superior when using coefficients determined with the linear regression method. Additionally, the exponential model performed best when trained using the simplex search method. Therefore, for the remaining trials in the current study only the results from the linear model trained using the linear regression method and the exponential model trained with the simplex method are shown.

6.3 Partial immersion results

While the models force predictions for full immersion operations were shown to be accurate to within 0.5 N, the end goal of these models is to predict the forces generated during finishing operations which tend to have lower MRR and consist primarily of partial immersion operations. Additionally, in full immersion passes the tool is fully constrained in the Y-axis by material on both sides, which is not the case for partial immersion cuts. To further validate the model a number of partial immersion tests were conducted to simulate material removal operations that are closer to the MRR found in finishing operations.

Figure 11 shows the setup for first set of partial immersion data, removing 0.1 *mm* from a 3 *mm* wide coupon. Figure 12 plots the mean measured force as hollow circles and the predicted forces using the linear and exponential models as '$+$' and '$\times$' respectively, all of which are plotted against the measured feed per tooth. The Y-axis force plot of Figure 12 demonstrates an interesting behaviour of

Table 2 Identified model parameters

	Linear model						Non-linear model			
	K_{rc}	K_{re}	K_{tc}	K_{te}	K_{ac}	K_{ae}	K_t	K_r	K_a	β
Linear Regression	1304.8	-1.1	1446.4	2.5	42.5	0.1	406.76	292.49	1.79	0.78
Simplex Search	1050.5	-0.1	1293.9	3.3	65.5	0.1	564.15	352.3	40.46	0.82

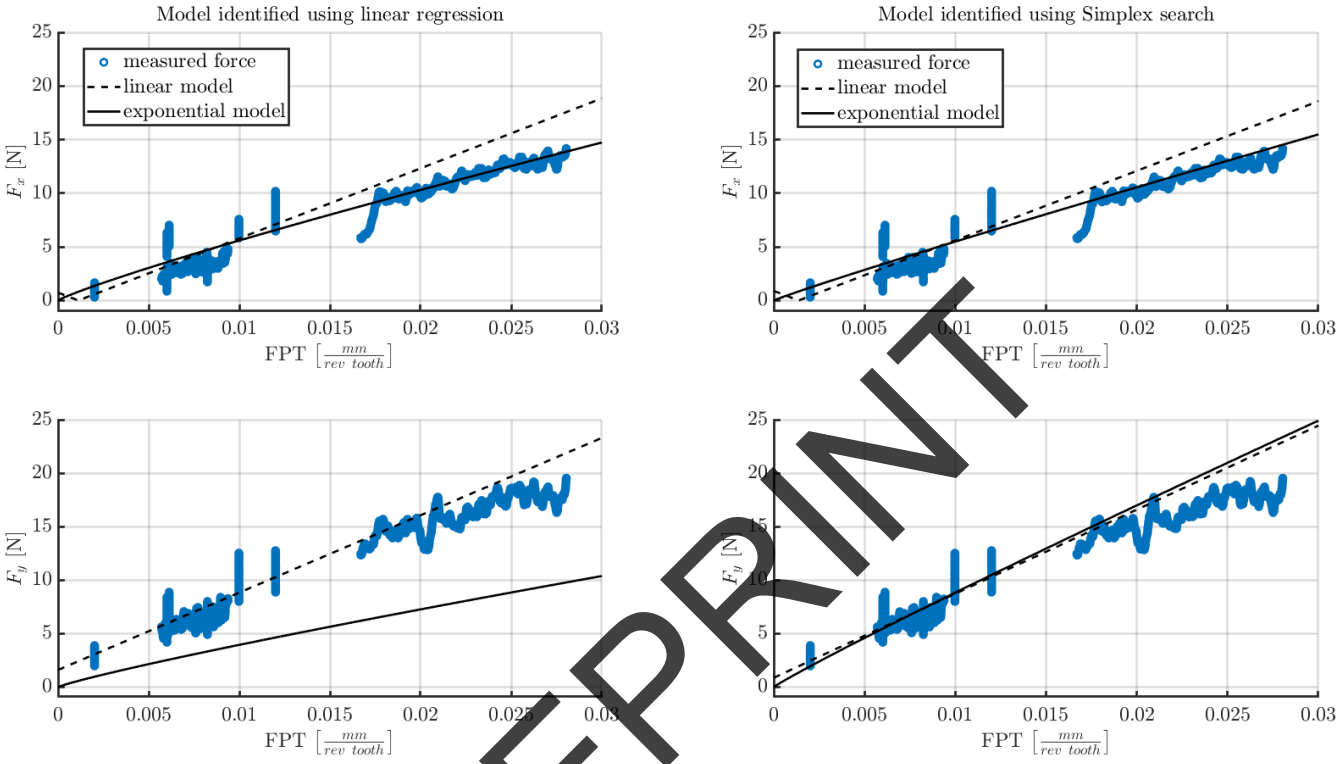

Fig. 9 Left: Measured data, linear and exponential model output vs. measured feed per tooth using models trained via regression method Right: Measured data, linear and exponential model output vs. measured feed per tooth using models trained via simplex search method

Table 3 Model performance summary: Force prediction accuracy

Model	Training	Mean force error $\pm$ 95%*CI*	
		X (N)	Y (N)
Linear	lin reg	0.41 $\pm$ 0.005	0.13 $\pm$ 0.003
Exponential	lin reg	0.17 $\pm$ 0.005	2.95 $\pm$ 0.006
Linear	Simplex Search	0.56 $\pm$ 0.005	0.41 $\pm$ 0.004
Exponential	Simplex Search	0.29 $\pm$ 0.005	0.54 $\pm$ 0.004

Table 4 Summary of predicted depth error

Model	Training	mean error (mm)
Linear	linear regression	-0.003 $\pm$ 0.1589
Exponential	linear regression	-0.116 $\pm$ 0.7075
Linear	Simplex search	-0.011 $\pm$ 0.1716
Exponential	Simplex search	0.035 $\pm$ 0.2540

the partial immersion passes, that the Y-axis forces do not increase with feed rate past 0.1 $\frac{mm}{rev \times tooth}$ and are generally much less sensitive to the changing feed rate than the X and Z-axis forces. This insensitivity to feed rate noted in the Y-axis forces matches the findings in Her [2] which found that the force along the Y-axis is much less sensitive to the overall MRR than the tangential force. The very low Y-axis forces created by this insensitivity to the feed rate are captured much more accurately by the exponential model.

Table 5 collects the average error with the 95% confidence interval and the standard deviation of the error for the values presented in Figure 12. The exponential model outperforms the linear model by 0.425 *N* in predicting the X-axis forces and 5.7 *N* in its predictions of the Y-axis forces.

A second set of partial immersion tests were conducted by removing a 0.8 *mm* by 0.5 *mm* simulated burr. A simulated burr was used in these tests in place of an actual burr as it provides a more consistent force profile to make comparing multiple trials easier, and, more importantly, it allows the models to be used as derived without additional processing, the application of these models to non-rectangular geome-

Table 5 Partial immersion force prediction accuracy (0.1×3 *mm* cut)

	X-axis error [N]		Y-axis error [N]		Z-axis error [N]	
	$\mu \pm$ 95% CI	σ	$\mu \pm$ 95% CI	σ	$\mu \pm$ 95% CI	σ
Linear	-0.72 $\pm$ 0.18	0.38	-0.57 $\pm$ 0.40	0.86	0.26 $\pm$ 0.058	0.38
Exponential	0.29 $\pm$ 0.039	0.082	-0.007 $\pm$ 0.068	0.15	0.23 $\pm$ 0.05	0.082

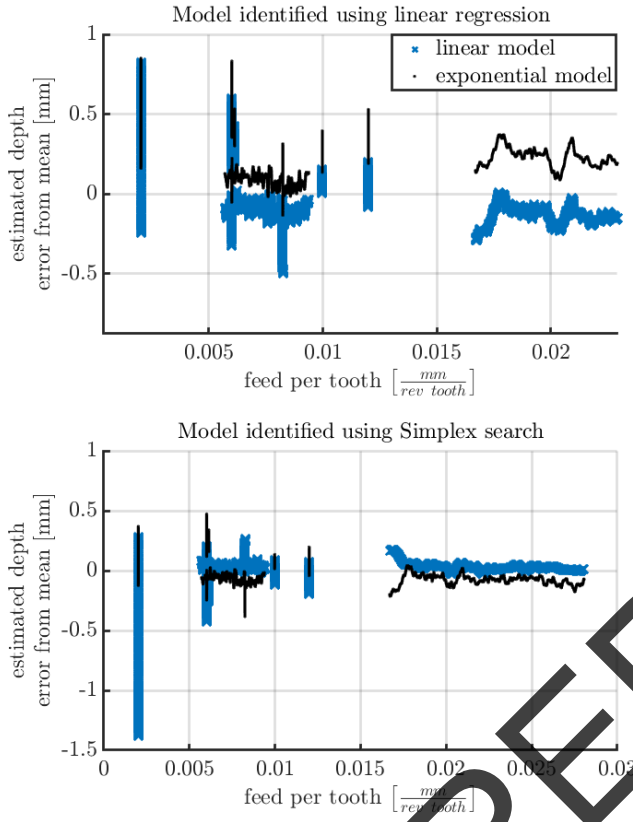

Fig. 10 Estimated error in depth prediction of linear and exponential models vs. measured feed per tooth

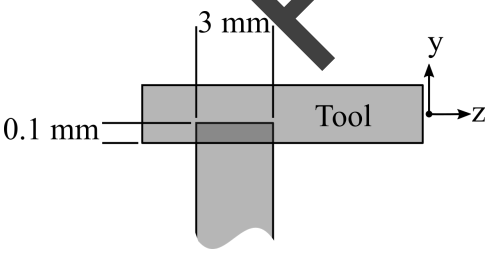

Fig. 11 Diagram of the 0.1×3 *mm* cut partial immersion cut. Linear feed along -X, tool rotation +Z

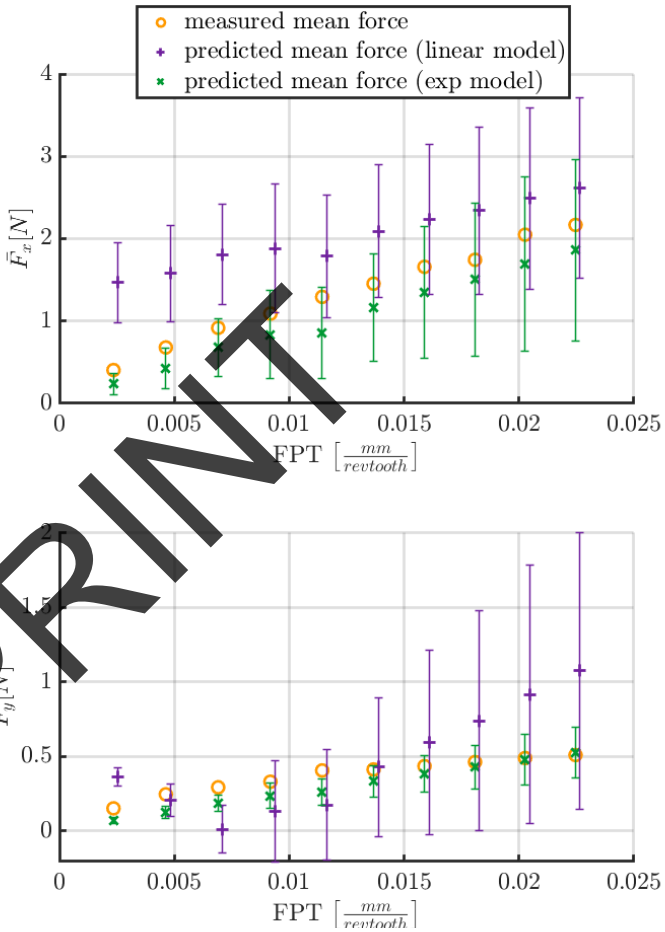

Fig. 12 Measured force vs. model prediction for partial immersion cut for 0.1×3 *mm* cut, error bars at 1σ. Linear model output shifted slightly along X-axis for readability.

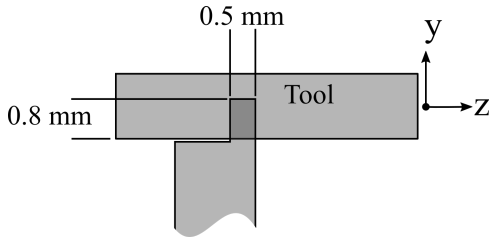

Fig. 13 Diagram of the 0.8×0.5*mm* cut partial immersion cut. Linear feed along -X, tool rotation +Z

tries is an area of further study. Figure 14 plots the mean measured force as hollow circles and the predicted forces using the linear and exponential models a stars an crosses respectively. The data in Figure 14 shows the exponential model is again better able to track the tangential force with a mean Y-axis error 1.5 *N* lower than the linear model.

6.4 Partial immersion depth prediction

The models were also used to estimate the depth of cut using the same technique used to obtain depth predictions for the full immersion tests. The exponential model has a mean

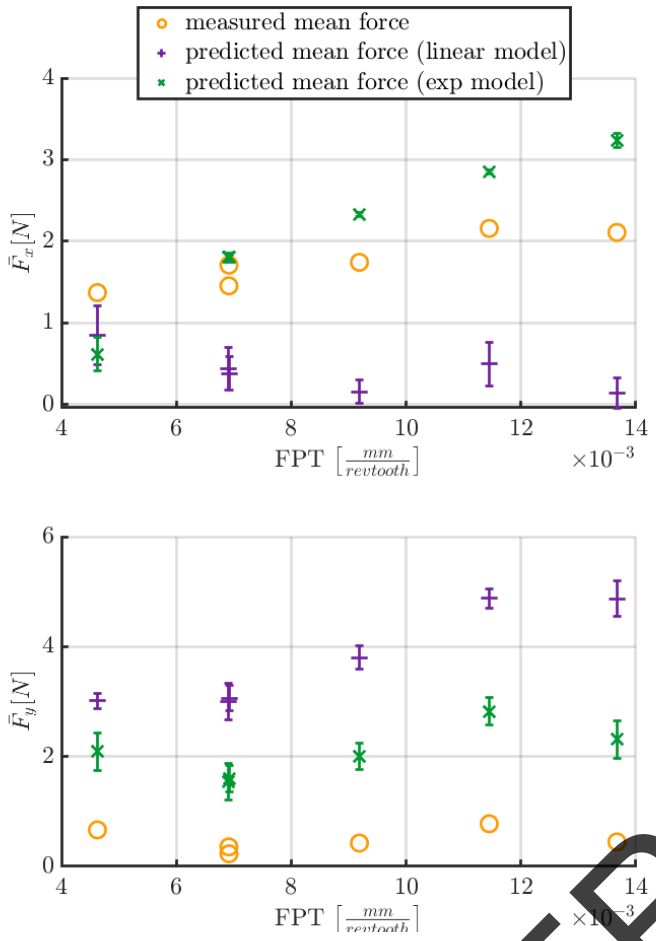

Fig. 14 Measured force vs. model prediction for partial immersion cut for $0.8 \times 0.5mm$ depth of cut, error bars at 1 σ

depth estimation error of 0.018 ± 0.017 which is nearly four times lower than that of the linear model with a mean error of 0.076 ± 0.022 *mm*. The exponential model tends to overestimate the depth of cut slightly, while the linear model consistently underestimates which follows the consistent over prediction of the contact force which seems to indicate that the linear model is unsuitable to modelling partial immersion processes.

7 Conclusion

This paper compared the performance of the linear force model proposed by Altintas and the exponential model proposed by Kienzle for low MRR milling operations. For the full immersion case, the linear model was four times more accurate, with a mean Y-axis error of 0.13 ± 0.003 *N* compared to the 0.54 ± 0.004 *N* error of the exponential model. However, in lower MRR partial immersion trials the exponential model was eighty times more accurate at predicting the cutting forces in along the Y-axis (-0.007 ± 0.0681 for the exponential vs. -0.572 ± 0.4009 for the linear.)

In addition to the contact force models, two methods to train the models were investigated: a linear regression based method proposed by Altintas [15] and a global search method proposed by Adem [16]. The models with parameters identified by the global search strategy produced a mean error across the X and Y-axes two times lower than the models whose parameters were identified by the linear regression method. The global search method was also more efficient when it comes to training as a wider range of feed rates and RPMs can be included in fewer tests.

The superior performance of the exponential model trained using the simplex search in the low MRR partial immersion case makes it the choice for future deburring model development. However, the linear model is still worth investigating further as it is significantly more computationally efficient which could prove crucial for online modelling tasks.

References

1. J. C. Aurich, D. Dornfeld, P. J. Arrazola, V. Franke, L. Leitz, and S. Min, "Burrs-Analysis, control and removal," *CIRP Annals - Manufacturing Technology*, vol. 58, no. 2, pp. 519–542, 2009.
2. M. G. Her and H. Kazerooni, "Automated Robotic Deburring of Parts Using Compliance Control," *Trans. of ASME J. of Dynamic Systems, Measurement, and Control*, vol. 113, no. 1, pp. 60–66, 1991.
3. F. Y. Hsu and L. C. Fu, "Intelligent robot deburring using adaptive fuzzy hybrid position/force control," *IEEE Transactions on Robotics and Automation*, vol. 16, no. 4, pp. 325–335, 2000.
4. E. Villagrossi, N. Pedrocchi, M. Beschi, L. Molinari, E. Villagrossi, N. Pedrocchi, and M. Beschi, "A human mimicking control strategy for robotic deburring of hard materials A human mimicking control strategy for robotic deburring of hard materials," *International Journal of Computer Integrated Manufacturing*, vol. 31, no. 9, pp. 869–880, 2018.
5. H.-c. Song and J.-b. Song, "Precision Robotic Deburring Based on Force Control for Arbitrarily Shaped Workpiece Using CAD Model Matching," vol. 14, no. 1, pp. 85–91, 2013.
6. M. E. Merchant, "Mechanics of the metal cutting process. I. Orthogonal cutting and a type 2 chip," *Journal of Applied Physics*, vol. 16, no. 5, pp. 267–275, 1945.
7. W. B. Palmer and P. L. B. Oxley, "Mechanics of Orthogonal Machining," *Proceedings of the Institution of Mechanical Engineers*, vol. 173, no. 1, pp. 623–654, 1959.
8. R. N. Roth and P. L. B. Oxley, "Slip-Line Field Analysis for Orthogonal Machining Based upon Experimental Flow Fields," *Journal of Mechanical Engineering Science*, vol. 14, no. 2, pp. 85–97, 1972.
9. N. Fang, I. S. Jawahir, and P. L. Oxley, "Universal slip-line model with non-unique solutions for machining with curled chip formation and a restricted contact tool," *International Journal of Mechanical Sciences*, vol. 43, no. 2, pp. 557–580, 2001.
10. Z. Han, H. Jin, and H. Fu, "Cutting force prediction models of metal machining processes: A review," *Proceedings of 2015 International Conference on Estimation, Detection and Information Fusion, ICEDIF 2015*, no. ICEDIF, pp. 323–328, 2015.
11. P. J. Arrazola and T. Özel, "Investigations on the effects of friction modeling in finite element simulation of machining," *International Journal of Mechanical Sciences*, vol. 52, no. 1, pp. 31–42, 2010.

12. M. Bäker, "Finite element simulation of high-speed cutting forces," *Journal of Materials Processing Technology*, vol. 176, no. 1-3, pp. 117–126, 2006.
13. F. Koenigsberger and A. Sabberwal, "An investigation into the cutting force pulsations during milling operations," *International Journal of Machine Tool Design and Research*, vol. 1, pp. 15–33, sep 1961.
14. Y. Altintas, A. Spence, and J. Tlusty, "End Milling Force Algorithms for CAD Systems," *CIRP Annals - Manufacturing Technology*, vol. 40, no. 1, pp. 31–34, 1991.
15. Y. Altintas, *Manufacturing automation : metal cutting mechanics, machine tool vibrations, and CNC design*. Cambridge University Press, 2012.
16. K. A. M. Adem, R. Fales, and A. S. El-Gizawy, "Identification of cutting force coefficients for the linear and nonlinear force models in end milling process using average forces and optimization technique methods," *International Journal of Advanced Manufacturing Technology*, vol. 79, no. 9-12, pp. 1671–1687, 2015.
17. M. Schwenzer, T. Auerbach, B. Döbbeler, and T. Bergs, "Comparative study on optimization algorithms for online identification of an instantaneous force model in milling," *International Journal of Advanced Manufacturing Technology*, vol. 101, no. 9-12, pp. 2249–2257, 2019.
18. M. Schwenzer, S. Stemmler, T. Bergs, and D. Abel, "Ensemble Kalman filtering for force model identification in milling," vol. 00, 2019.
19. U. Thombansen, G. Buchholz, D. Frank, J. Heinisch, M. Kemper, T. Pullen, V. Reimer, G. Rotshteyn, M. Schwenzer, S. Stemmler, D. Abel, T. Gries, C. Hopmann, F. Klocke, R. Poprawe, U. Reisgen, and R. Schmitt, "Design framework for model-based self-optimizing manufacturing systems," *International Journal of Advanced Manufacturing Technology*, vol. 97, no. 1-4, pp. 519–528, 2018.
20. M. Wan and W. H. Zhang, "Systematic study on cutting force modelling methods for peripheral milling," *International Journal of Machine Tools and Manufacture*, vol. 49, no. 5, pp. 424–432, 2009.
21. E. Budak, Y. Altintaş, and E. J. Armarego, "Prediction of milling force coefficients from orthogonal cutting data," *Journal of Manufacturing Science and Engineering, Transactions of the ASME*, vol. 118, no. 2, pp. 216–224, 1996.
22. O. Kienzle, "Die bestimmung von kräften und leistungen an spanenden werkzeugen und werkzeugmaschinen," *VDI-Z*, vol. 94, no. 11-12, pp. 299–305, 1952.
23. M. Y. Tsai, S. Y. Chang, J. P. Hung, and C. C. Wang, "Investigation of milling cutting forces and cutting coefficient for aluminum 6060-T6," *Computers and Electrical Engineering*, vol. 51, pp. 320–330, 2016.